



Deposition of nanocomposite Cu–TiO₂ using heterogeneous colliding plasmas

Pramod K. Pandey^{1,2} · Raj K. Thareja³ · Ravi Pratap Singh^{3,4} · John T. Costello¹

Received: 23 August 2017 / Accepted: 16 February 2018 / Published online: 21 February 2018
© Springer-Verlag GmbH Germany, part of Springer Nature 2018

Abstract

The formation of CuTiO₂ nanocomposites has been observed in an experiment in which laser plasma plumes of Cu and Ti collide and stagnate in an oxygen atmosphere. The inherent advantage of this technique lies in its simplicity and flexibility where laser, target composition and geometry along with ambient atmosphere are all controllable parameters through which the stoichiometry of the deposited nanocomposites may be selected. The experiment has been performed at three oxygen ambient pressures 10⁻⁴, 10⁻², 10⁰ mbar and we observe its effect on stoichiometry, and morphology of the deposited nanocomposites. Here, we show how the stoichiometry of deposited nanocomposites can be readily controlled by changing just one parameter, namely the ambient oxygen pressure. The different peaks of photoluminescence spectra $\lambda = 390$ nm ($E = 3.18$ eV) corresponding to the anatase phase of TiO₂, along with the peaks at $\lambda = 483$ nm ($E = 2.56$ eV) and 582 nm ($E = 2.13$ eV) of deposited nanocomposites, shows the doping/blending effect on the band gaps which may potentially be of value in solar cell technology. The technique can, in principle, be extended to include nanocomposites of other materials making it potentially more widely applicable.

1 Introduction

Pulsed laser deposition (PLD) of materials in a background gas is an extensively used technique for thin film growth, nanoparticle production and nano-structuring of surfaces [1, 2]. The structural morphology of the nanocrystals formed is shown to be highly dependent on the plasma plume expansion dynamics and plasma species collision with the ambient gas. It has been reported that not only collisions with the ambient gas but also collisions with another plume help to form nanocrystalline materials [3]. Further, colliding plasma plumes in ambient gases not only provide more controlled

formation of nanoparticles/nanocrystalline materials but can indirectly help to enhance the limit of detection (LOD) in elemental analysis [4, 5].

The main motivation for the present work is that the method of colliding plasma plumes originating from two different target materials, as discussed by Umezu et al. [3, 6], could be used in crystalline nanocomposites (here CuTiO₂) formation and deposition with a slight modification in the target geometry. We note here for completeness that the crossed beam pulsed laser deposition method has been used by Tselev et al. [7–10] to mitigate the debris and particulates from the collisional zone in the context of film growth. Similar work has been reported in [11] where ArF (193 nm) and frequency tripled Nd:YAG (355 nm) lasers irradiating TiO₂ and Au targets, respectively, in oxygen at a pressure of 30 Pa were used to deposit Au–TiO₂ nanocomposites. Also, work on colliding species by Voevodin et al. [12] involves the combination of magnetron sputtering and pulsed laser deposition as a hybrid technique in which the plasma fluxes intersect on the substrate surface. Other methods such as the photocatalytic reduction technique [13] are based on specific chemicals for preparing nanocomposites which are different for different nanocomposite materials. On the other hand, our heterogeneous colliding plasma deposition (HCPD) method, which involves the collision of plasmas to drive

✉ Pramod K. Pandey
panditpkp@gmail.com; ppandey@iitk.ac.in

¹ National Centre for Plasma Science and Technology and School of Physical Sciences, Dublin City University, Dublin 9, Ireland

² Present Address: Centre for Lasers and Photonics and Photonics Sciences and Engineering Programme, Indian Institute of Technology Kanpur, Kanpur, India

³ Department of Physics, Indian Institute of Technology Kanpur, Kanpur, India

⁴ Present Address: Department of Applied Science, Madan Mohan Malviya University of Technology, Gorakhpur, India

plasma chemistry at the collision plane, leaves the plasma stagnation layer with the possibility to react with ambient gases.

In contrast to György et al. [11] we employ only elemental (metal) targets in an ambient gas. This is a simple system, capable of producing a rich array of nano-objects, with a great deal of potential due to its ease of set up and the fact that there is no sample preparation needed. Nanocrystalline-titanium dioxide (TiO_2) is rapidly becoming a wide spread used material due to its wide range of applications in e.g., light to electrical energy conversion and storage and also photo-catalysis [14–16]. However, its wide band gap (3.0–3.2 eV) restricts its applicability to the UV absorption range. This is a severe limitation, especially in photovoltaic applications and visible light photo-catalysis. Several efforts to extend strong phototabsorption by TiO_2 into the visible spectral range have been reported in the recent past such as compositional variation to make suboxides [18], surface modification [19] and doping [10–21]. Among all these methods, material doping of the host TiO_2 appears to be the most promising approach for band-gap tailoring in the visible range. Several methods have been reported for the doping of Cu, Co, V and Fe to enhance the absorption of visible light [20–23]. However, the major challenge is to provide a low cost, more effective method, which is well controlled and sufficiently versatile so that it can produce the desired photoabsorption properties for TiO_2 .

We present here a relatively simple and potentially very versatile method for the deposition of nanocomposites using HCPD. Compared to conventional pulsed laser deposition, HCPD provides greater flexibility in the sense that not only are two (or more if desired) simple metal plasma plumes involved but the individual plume parameters (e.g., temperature, density, ionization and excitation balance) can be independently controlled by choice of laser parameters. Furthermore, the physics and chemistry at the collision plane can be tailored by choice of target geometry as well as ambient gas type and pressure to achieve a specific desired stoichiometric composition of the nanocomposites formed. Importantly, no pre-preparation of the target materials and ambient gas is required, rather only pure solid samples of, in the case of the experiments reported here, titanium, copper and oxygen gas are required. The present work is organized into four sections. Section 2 gives the details of the experimental setup; details of the results and discussion are given in Sect. 3 and conclusions are presented in Sect. 4.

2 Experimental

We used a nanosecond Nd:YAG laser (Quanta Ray INDI) with a pulse width $\tau_p = 8$ ns (full width at half maximum, FWHM) at a pulse repetition rate of 10 Hz, operated at its

fundamental wavelength ($\lambda = 1064$ nm) to create heterogeneous colliding plasmas in oxygen ambient. The target comprised concentric rings of Cu and Ti onto which two laser beams, obtained by splitting a single beam using a wedge prism, were focused, one onto the Cu surface and the other onto the Ti surface. The intensity of each laser beam on the target surface was kept at 9 GW/cm^2 . The distance between the two focal spots was 2.0 mm and angle of incidence of the laser beam was 45° with respect to the target surface. For deposition of nanocomposites we placed the substrate holder 4.0 cm away from the target surface and the deposition time was 3 h.

To observe plume dynamics within the colliding plasma system, we used a gated intensified charged coupled device (Andor Model No. DH-720) which was synchronised to the optical laser pulse with a jitter of ± 1 ns. A plane mirror combined with a zoom lens system was used to image the plasma onto the ICCD. A field emission scanning electron microscope (FESEM) (JXA 8230, JEOL) was used to observe the morphology of the deposited structures. It could also perform energy-dispersive X-ray spectroscopy (EDX) to measure the stoichiometry of the deposited structures. The structural properties of the deposited nanocomposites were investigated by X-ray diffraction (Panalytical X-ray Pro MRD) using the Cu $K\alpha$ line (0.1541 nm). The optical properties were investigated using photoluminescence (PL) with an excitation wavelength $\lambda_{\text{ex}} = 355$ nm (Fluorolog (R)-3 Jobin Yvon Horiba). A schematic diagram of the colliding plasma deposition setup is shown in Fig. 1.

3 Results and discussions

The images of expanding copper and titanium plasma plumes shown in Fig. 2 were recorded at 10^{-4} , 10^{-2} and 10^0 mbar oxygen ambient. The time delays shown on the figure are with respect to the ablating laser pulse. The copper and titanium plasma plumes expand linearly before colliding with each other at 10^{-4} and 10^{-2} mbar-ambient pressures whereas at 10^0 mbar, the expansion of the each plasma plume follows the drag force model [24]. Further, since copper is heavier than titanium, the copper species move at a lower average velocity than the titanium species. The mass ratio is given by $\left(\frac{m_{\text{Cu}}}{m_{\text{Ti}}} = 1.3\right)$, where m_{Cu} and m_{Ti} are the copper and titanium-atomic masses, respectively.

Hence, at 10^{-4} mbar oxygen ambient, a high proportion of the titanium-atomic species escape from the target surface and transit past the collision plane before a sufficient number of Cu atomic species reach the plane, thereby allowing stagnation to begin. As the ambient pressure is increased to 10^{-2} mbar, the seed plasma plumes become more confined and the difference in velocity between the two plumes is reduced.

Fig. 1 Schematic of the experimental setup

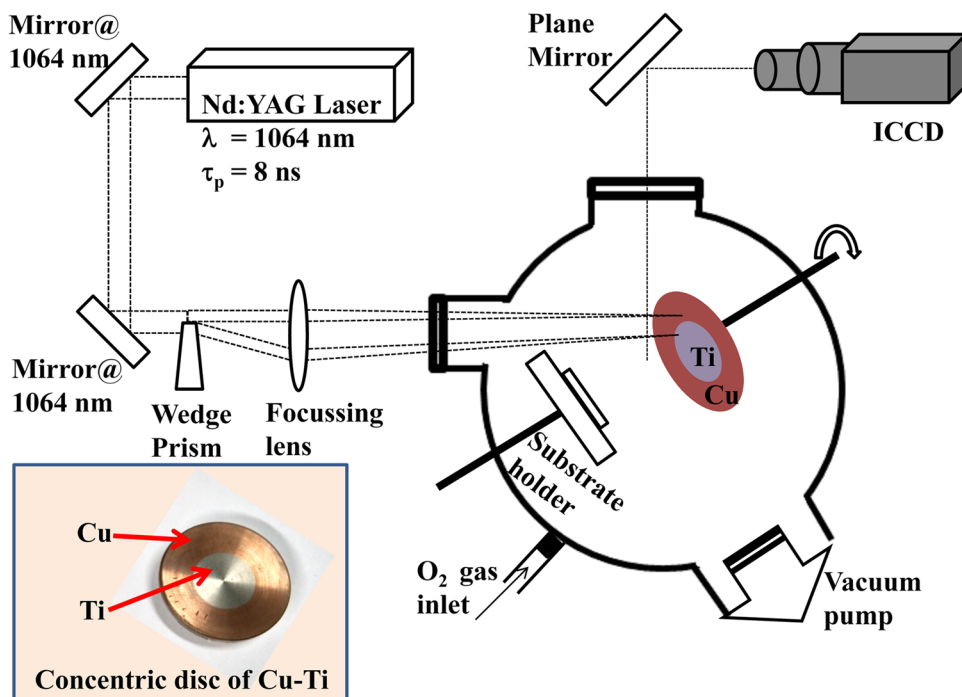
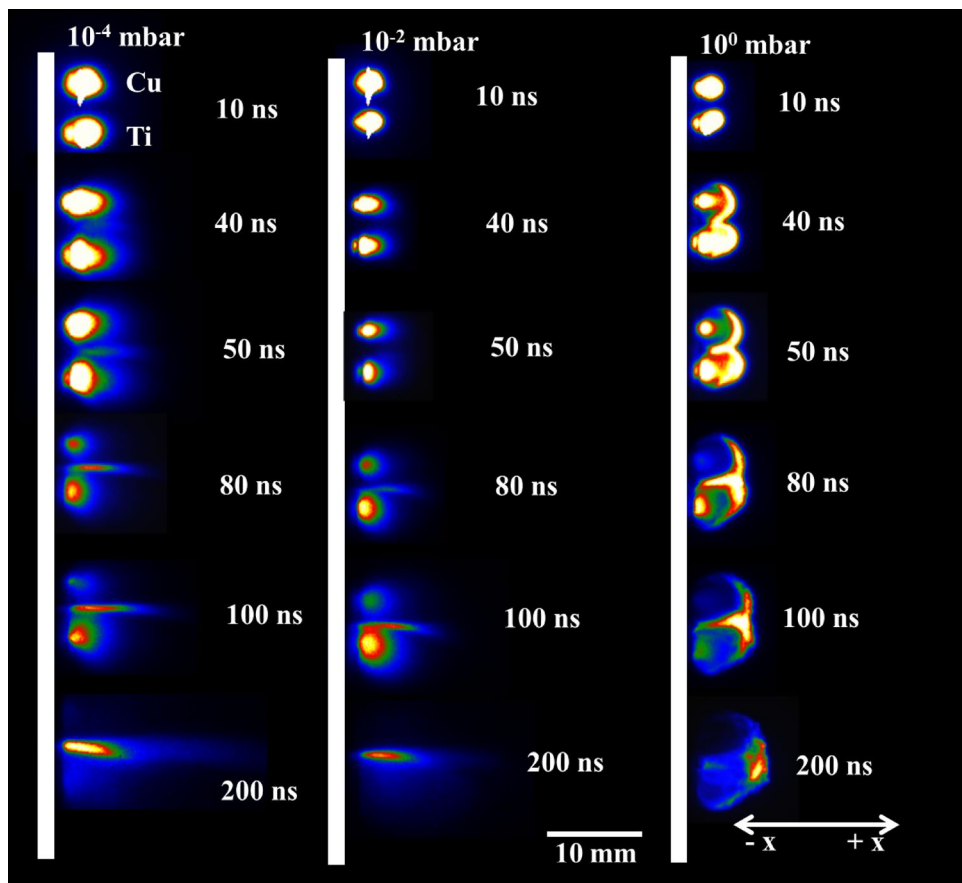


Fig. 2 ICCD images of expanding copper and titanium plasmas showing stagnation at oxygen ambient pressures of 10⁻⁴, 10⁻², and 10⁰ mbar



This has two consequences. First, a higher proportion of the ablated Ti species are now available to collide with Cu species and participate in stagnation layer formation at the collision plane. Second, the stagnation layer starts to form later in the higher pressure case as the plumes are moving more slowly due to the increased confinement.

At 10^0 mbar-ambient pressure, it can be seen from Fig. 2 that the front edges of the Cu and Ti seed plumes exhibit quite a degree curvature early on in their evolution. As time progresses, they appear to start to turn back (i.e., propagate in negative x -direction) on each other to form a bright layer of emitting material that propagates backwards (negative

x -direction) along the collision plane towards the target surface (see images at delays of 40 and 50 ns). As time progresses, further the plume fronts begin to flatten as the fast-moving species normal to the target surface slow down and the species moving along off axis directions catch up (see images at time delays of 80 and 100 ns). From time-space resolved spectroscopy [24] we can state that the bright emission at the collision plane is not due to confined oxygen species trapped by the expanding seed plumes, but rather originates from ablated material.

Figure 3 shows the field emission scanning electron microscope (FESEM) images and corresponding

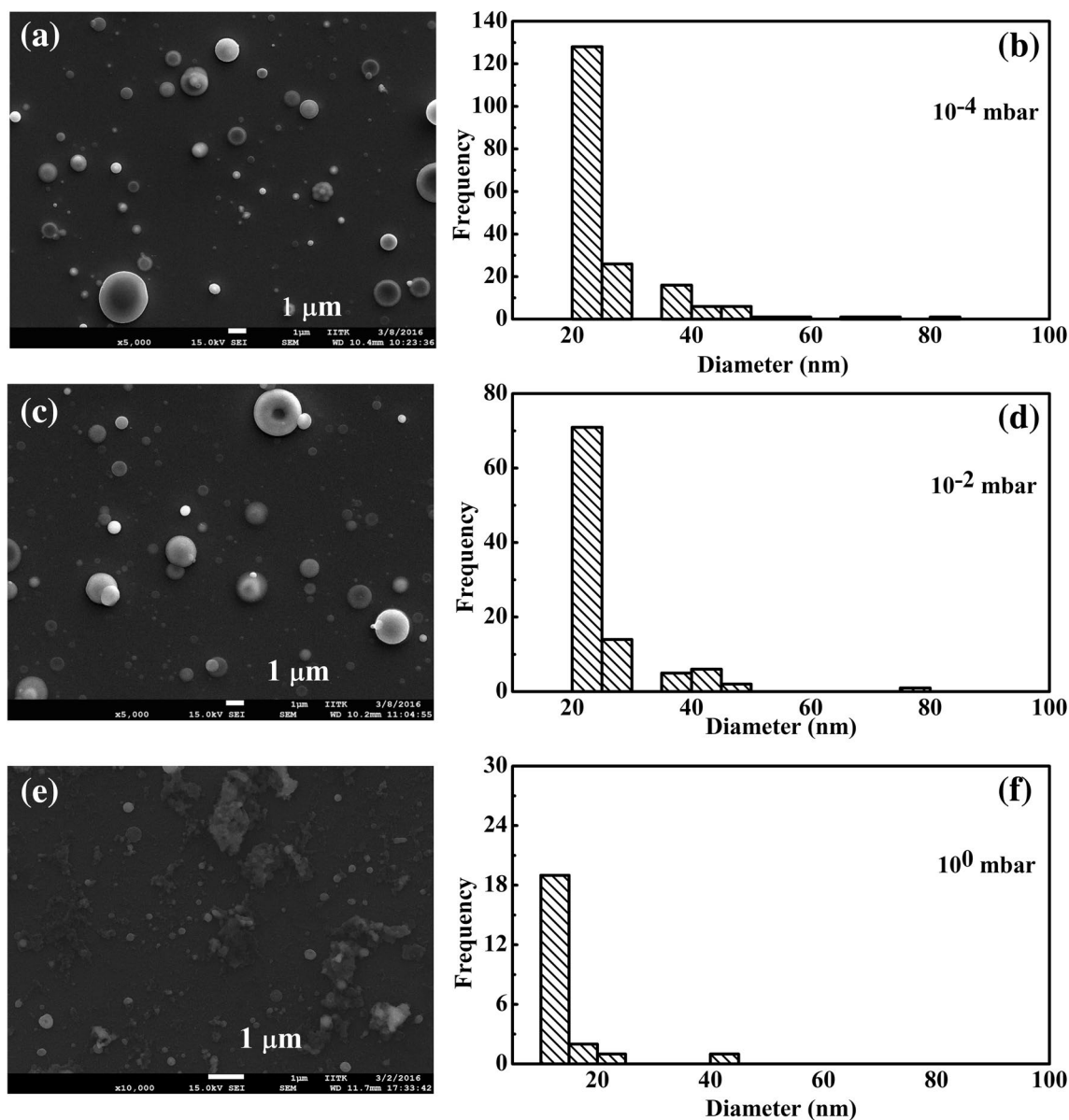


Fig. 3 FESEM images and their corresponding particle distributions of the deposited material **a, b** at 10^{-4} mbar, **c, d** at 10^{-2} mbar, and **e, f** at 10^0 mbar

particle size distributions of the deposited nanocomposites (Cu-TiO₂) on silicon substrates which were placed at a distance of 4 cm from the target surface in ambient oxygen pressures of 10⁻⁴, 10⁻², and 10⁰ mbar, respectively. Figure 3a, b show the FESEM images and corresponding particle size distributions with a large number of particles formed that possess a diameter in the range of 20–30 nm at

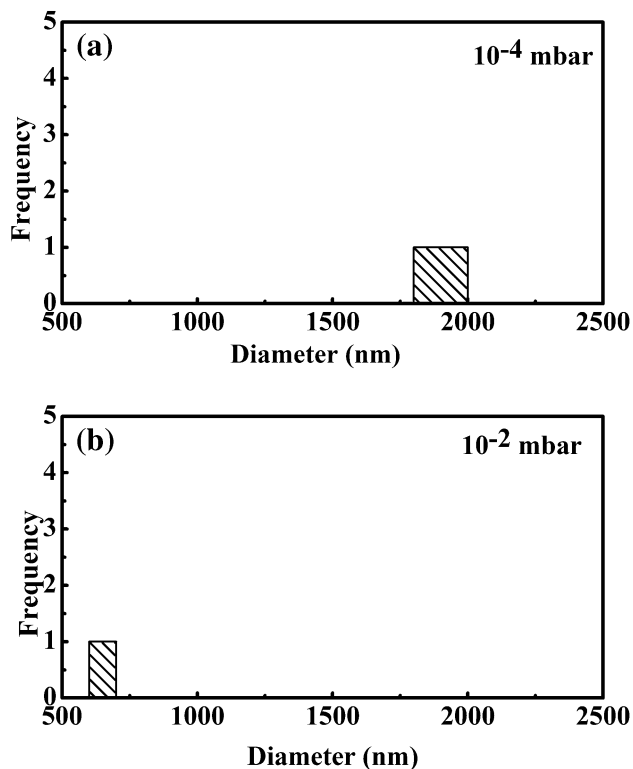


Fig. 4 Particle distributions of the deposited material at larger scale **a** at 10⁻⁴ mbar and **b** at 10⁻² mbar

10⁻⁴ mbar. At 10⁻² mbar, (cf. Fig. 3c, d) the particle sizes and their distribution are found to be similar to 10⁻⁴ mbar, albeit they have a lower abundance due to the plume confinement near to the target surface (hence comparatively fewer nanoparticles reach the substrate). On the other hand, at 10⁰ mbar (cf. Fig. 3e, f) the plasma plume dynamics changes and flattening of the stagnation layer front is initiated which reduces the nanoparticle flux moving directly towards the substrate. It is also noticeable that the nanoparticle sizes become smaller because at higher pressure enhanced collisional events between the plasma species reduce the agglomeration rate.

Figure 4a, b show an abundance of micro-particles with an average particle size ~ 1.8 μm at 10⁻⁴ mbar and ~ 650 nm at 10⁻² mbar which are not shown in Fig. 3 due to scaling. In Fig. 3a, c we observe the presence of rare donut-shaped structures and its magnified view is shown in Fig. 5. We cannot be definitive as to the mechanism but one possibility is that they arise from TiO₂ nanotubes or other elongated nanostructures that deteriorate in the presence of Cu and collapse to form donuts [25].

The FESEM used (JXA 8230, JEOL) could also perform energy-dispersive X-ray spectroscopy (EDX) as stated above. Using this technique, the stoichiometric concentration of copper, titanium and oxygen is found to be Cu 70.6 wt%, Ti 19.9 wt% and O 9.5 wt% at 10⁻⁴ mbar. On the other hand at 10⁻² mbar it becomes Cu 35 wt%, Ti 33 wt% and O 32 wt% and at 10⁰ mbar it is Cu 11.2 wt%, Ti 6.2 wt% and O 11.2 wt% and the remainder represents the contribution of the silicon substrate. Although the overall abundance of nanoparticles reaching the substrate is reduced at 10⁻² mbar, the relative concentration of Ti and O is increased with respect to copper (which is concomitantly reduced) and this corroborates the ambient pressure effect on atomic mobilities and resultant concentrations at the collisional

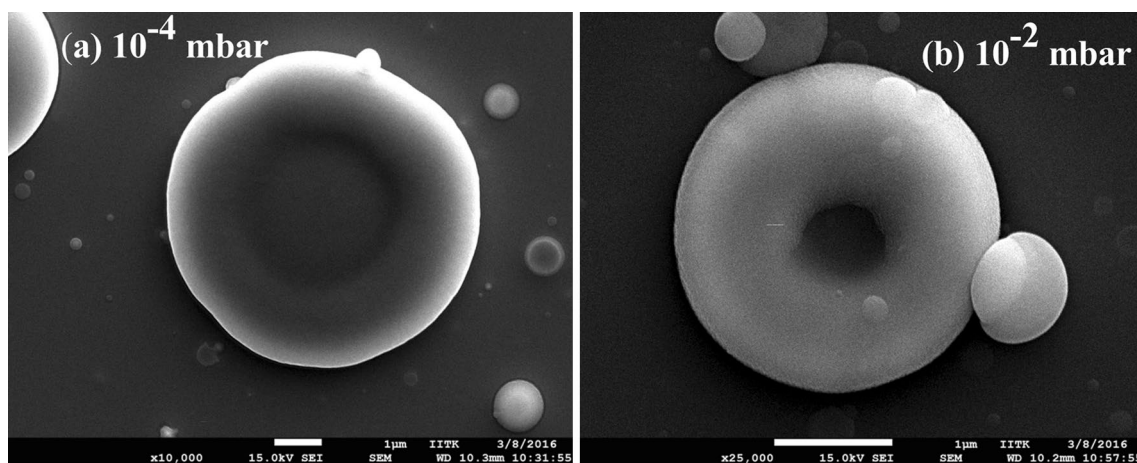
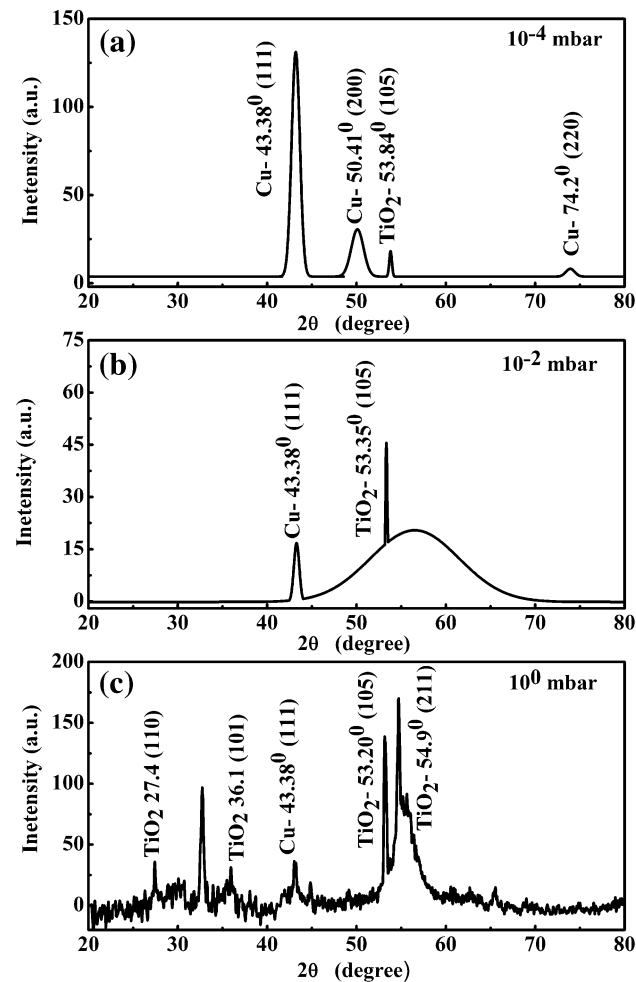


Fig. 5 Magnified view of rare donut-shaped structures **a** at 10⁻⁴ mbar and **b** at 10⁻² mbar

Table 1 Stoichiometric concentration of Cu, Ti, and O in deposited structures at different pressures

Ambient pressure (mbar)	Cu wt%	Ti wt%	O wt%
10^{-4}	70.6	19.9	9.5
10^{-2}	35	33	32
10^0	11.2	6.2	11.2

**Fig. 6** X-ray diffraction peaks of the deposited nanocomposites (CuTiO₂) **a** at 10^{-4} mbar, **b** at 10^{-2} mbar and **c** at 10^0 mbar

plane as discussed earlier. Table 1 shows the stoichiometric concentration of Cu, Ti, and O in deposited structures at different pressures as discussed above.

Figure 6a–c show the corresponding X-ray diffraction (XRD) peaks of the deposited material shown in Fig. 3a, c, and e, respectively. The XRD pattern of the deposited nanocomposites at 10^{-2} mbar in Fig. 6b shows the Cu peak at 43.38° (111) along with the TiO₂ anatase phase peak at 53.35° (105) (sitting on top of a broader feature). On the

other hand, at 10^{-4} mbar, only sharp Cu peaks at 43.38° (111) and a TiO₂ anatase phase peak at 53.84° (105) are observed [2, 26, 27]. The shift in the peak position to a higher diffraction angle at 10^{-4} mbar is due to an enhanced dopant (copper) concentration [26]. However, at 10^0 mbar-ambient pressure Cu peaks at 43.38° (111), TiO₂ anatase phase peaks at 53.20° (105), 54.9° (211) and rutile phase peaks at 27.4° (110) and 36.1° (101) are observed [27]. The XRD peaks confirm that at 10^{-4} mbar, where the copper concentration (dopant) is higher than titanium, the CuTiO₂ nanocomposite is crystalline in nature and exists within the anatase phase of TiO₂. On the other hand, at 10^{-2} mbar where the copper concentration has dropped to approximately the same value as the titanium concentration, the broad peak indicates that the crystallinity of the deposited nanocomposites has been considerably reduced. However, the narrow peak sitting atop the broad peak indicates that the TiO₂ anatase phase survives. The abundance of rutile and anatase phase peaks at 10^0 mbar may be due to the enriched oxygen-ambient atmosphere during deposition.

To obtain further confirmation, we used the XRD Cu peak at 43.38° (111) along with the TiO₂ anatase phase peaks at 53.84° , 53.35° and 53.20° (105) and the rutile phase peak at 27.4° (110) obtained variously at ambient pressures of 10^{-4} and 10^{-2} , and 10^0 mbar to calculate the crystallite size using the Debye–Scherrer formula ($D = \frac{0.94 \lambda}{\beta \cos \theta}$) where

D is the average crystallite size, λ is Cu K α wavelength (0.1541 nm), β is the FWHM of the considered XRD peak and θ , is the Bragg diffraction angle [25, 28]. The calculated crystallite size, $D = 27.4$ nm, using the peak at 53.84° at 10^{-4} mbar pressure is comparable to the reported value [25] of $D = 28.2$ nm. The difference between the two values may be due to slightly different concentrations of copper.

At 10^{-2} mbar pressure, the crystallite size is increased to $D = 46.4$ nm. The calculated crystal size at 10^0 mbar anatase phase is $D = 26.6$ nm and for rutile phase it is $D = 53.4$ nm, comparable to the reported value [29] of $D = 52$ nm. The crystal spacing [28] ($d = \frac{\lambda}{2 \sin \theta}$) where λ is Cu K α wave-

length (0.1541 nm) and θ is the Bragg diffraction angle remains unchanged at $d = 0.170$ nm and calculated lattice constants are $a = b = 0.378$ nm and $c = 0.951$ nm [25] for the anatase phase at all the pressures on the other hand, the calculated crystal spacing for rutile phase is found to be $d = 0.325$ nm and lattice constants are $a = b = 0.459$ nm and $c = 0.296$ nm [30]. This surprising result may be due to the similarity in ionic radius of Cu²⁺ (0.073 nm) and Ti⁴⁺ (0.064 nm) ions which enables Cu²⁺ to replace Ti⁴⁺ leaving no change in crystal spacing of the anatase phase TiO₂ [26]. However, the enhanced oxygen vacancy concentration could lead to the formation of CuO monomers which condense on the existing CuTiO₂ particles in such a way as to enhance

the crystallite size in directions other than the crystal spacing leading to the rutile phase. This in turn results in a decrease in the particle crystallinity and an increase in the amount of amorphous material, preventing grain growth [26, 31]. Hence, we conclude that excess oxygen in the deposition chamber reduces the crystallinity of the nanocomposites.

Figure 7 shows the photoluminescence (PL) spectra of the deposited nanocomposites. The PL spectra were recorded using an excitation wavelength $\lambda_{\text{ex}} = 355$ nm. The observed PL spectra for all samples show the same PL peaks at $\lambda = 390$ nm ($E = 3.18$ eV) corresponding to the anatase phase of TiO₂ and peaks at $\lambda = 483$ nm ($E = 2.56$ eV) and 582 nm ($E = 2.13$ eV) which occur due to surface states of Ti⁴⁺-OH [32] and copper, respectively, because it introduces new energy levels of Cu²⁺/Cu⁺ into the TiO₂ band gap [32–34]. The new energy levels introduced by Cu²⁺/

Cu⁺ ions in TiO₂, yield new PL peak at $\lambda = 582$ nm, along with pure TiO₂ peaks, because of electron transfer from the conduction band of TiO₂ to the new level introduced by copper ions [32].

The increased concentration of oxygen at 10⁻² mbar pressure, leading to faster formation of CuO compared to CuTiO₂, leads in turn to a slight reduction in the intensity of the PL peaks. This happens because copper, with an electronegativity of 1.90, is more electronegative than titanium (relative electronegativity 1.54) [35] and thus, in the presence of excess oxygen, CuO monomer formation reduces crystallinity and hence the PL intensity. The absence of a PL peaks at 10⁰ mbar corresponding to the rutile phase TiO₂ $\lambda = 413.28$ nm ($E = 3.0$ eV) may be due to its lower abundance. However, the enhanced PL peak intensity (cf. Fig. 7c) is due to the abundance of smaller nanoparticles (10–20 nm) which leads to a strong surface plasmon resonance resulting in strong emission [2]. The presence of nanoparticles with PL peaks at 2.56 and 2.13 eV other than 3.18 for pure TiO₂ shows that nanocomposites deposited with this method could be better suited for applications in solar cell technology because these particles can absorb photons in the UV to visible range and a concomitant increase in solar cell conversion efficiency [36].

4 Conclusions

The potential of the heterogeneous colliding plasma method for the deposition of composite nanoparticles (CuTiO₂) is demonstrated. We have shown that the stoichiometry of the deposited material can be controlled by controlling the ambient pressure. Study of crystal lattice parameters shows that anatase phase deposition of CuTiO₂ can be controlled by ambient gas pressure because at higher ambient pressure, (10⁰ mbar) the rutile phase signature begins to appear. A photoluminescence study of the deposited structure and effect of plasmon resonance on PL intensity shows that judicious pressure-controlled deposition of composite nanoparticles could be useful for applied or possibly even industrial purposes. This method of deposition also provides several other parameters to control the stoichiometry and the morphology of the composite nanoparticles such as the laser pulse energy, wavelength, and pulse duration, distance between the two seed plasmas, focal spot size, etc.

Acknowledgements Work supported by Science Foundation Ireland under Grant Nos. 12/IA/1742 and 16/RI/3696. We acknowledge EU FP7 Grant Agreement No. 318941 under the project “Ultrafast Photonics-Processes and Interactions (UP-PI)” for travel funds. Pramod Pandey acknowledges support under the EU FP7-PEOPLE-2013-IIF Programme, Grant Agreement No. 628789. This work is associated with the FP7 EU COST Action MP1208 and the US National Science Foundation PIRE Grant No. 1243490.

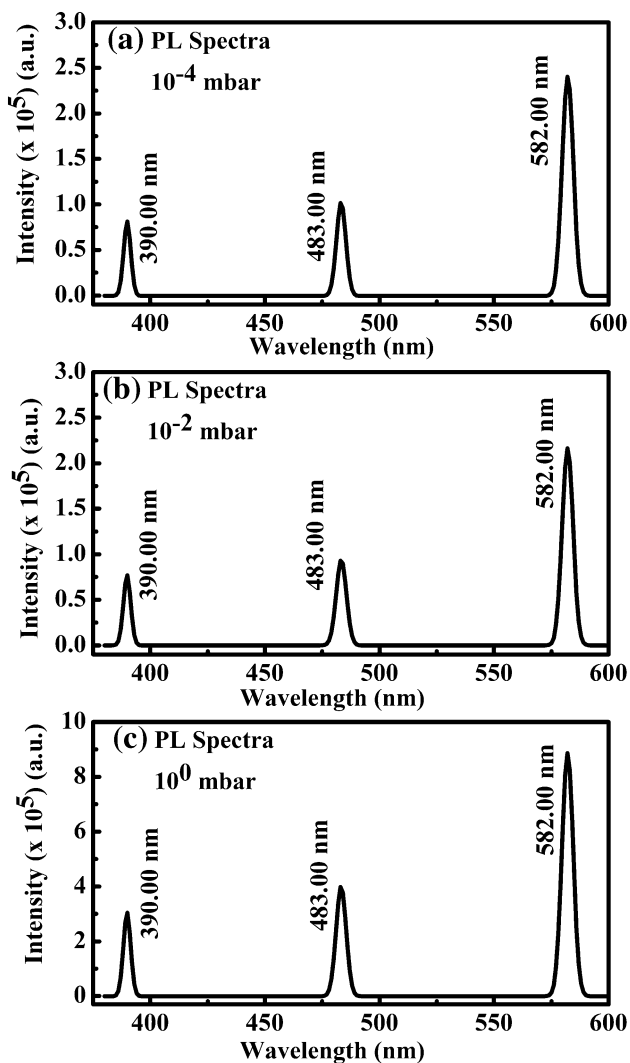


Fig. 7 Photoluminescence spectra of the deposited nanocomposites

References

1. T. Szorenyi, Z. Geretovszky, *Thin solid films*. **453–454**, 431 (2004)
2. P.K. Pandey, R.K. Thareja, *Phys. Plasmas*. **18**, 033505 (2011)
3. I. Umezu, S. Yamamoto, A. Sugimura, *Appl. Phys. A*. **101**, 133 (2010)
4. C. Koral, A. De Giacomo, X. Mao, V. Zorba, R.E. Russo, *Spectrochim. Acta B*. **125**, 11 (2016)
5. H. Luna, K.D. Kavanagh, J.T. Costello, *J. Appl. Phys.* **101**, 033302 (2007)
6. I. Umezu, N. Sakamoto, H. Fukuoka, Y. Yokoyama, K. Nobuzawa, A. Sugimura, *Appl. Phys. A*. **110**, 629 (2013)
7. A. Tselev, A. Gorbunov, W. Pompe, *Rev. Sci. Instrum.* **72**, 2665 (2001)
8. M.D. Strikovsky, E.B. Klyuenkov, S.V. Gaponov, J. Schubert, C.A. Copetti, *Appl. Phys. Lett.* **63**, 1146 (1993)
9. C. Sánchez Aké, R. Sanginés, H. de Castro, M. Sobral, Villagrán-Muniz, *J. Appl. Phys.* **100**, 053305 (2006)
10. A. Tselev, A. Gorbunov, W. Pompe, *Appl. Phys. A*. **69**, 353 (1999)
11. E. György, G. Sauthier, A. Figueras, A. Giannoudakos, M. Kompitsas, I.N. Mihailescu, *J. Appl. Phys.* **100**, 114302 (2006)
12. A.A. Voevodin, M.A. Capano, A.J. Safriet, M.S. Donley, J.S. Zabinski, *Appl. Phys. Lett.* **69**, 188 (1996)
13. S. Chen, Y. Guo, S. Chen, Z. Ge, H. Yang, J. Tang, *Mater. Lett.* **83**, 154 (2012)
14. P.V. Kamat, *J. Phys. Chem. Lett.* **2**, 839 (2011)
15. X. Chen, A. Selloni, *Chem. Rev.* **114**, 9281 (2014)
16. I.B. Gosbell, *Am. J. Clin. Dermatol.* **5**, 239 (2004)
17. H. Tong, S. Ouyang, Y. Bi, N. Umezawa, M. Oshikiri, J. Ye, *Adv. Mater.* **24**, 229 (2012)
18. S.Y. Dhumal, T.L. Daulton, J. Jiang, B. Khomami, P. Biswas, *Appl. Catal. B*. **86**, 145 (2009)
19. L.P. Li, J.J. Liu, Y.G. Su, G.S. Li, X.B. Chen, X.Q. Qiu, T.J. Yan, *Nanotechnol.* **20**, 155706 (2009)
20. R. Asahi, T. Morikawa, T. Ohwaki, K. Aoki, Y. Taga, *Science*. **293**, 269 (2001)
21. W.Y. Choi, A. Termin, M.R. Hoffmann, *J. Phys. Chem.* **98**, 13669 (1994)
22. W. Li, Y. Wang, H. Lin, S.I. Shah, C.P. Huang, D.J. Doren, S.A. Rykov, J.G. Chen, M.A. Barteau, *Appl. Phys. Lett.* **83**, 4143 (2003)
23. K.S. Rane, R. Mhalsiker, S. Yin, T. Sato, K. Cho, E. Dunbar, P. Biswas, *J. Solid. State. Chem.* **179**, 3033 (2006)
24. P.K. Pandey, R.K. Thareja, J.T. Costello, *Phys. Plasmas*. **23**, 103516 (2016)
25. S.H. Kim, S.-Y. Choi, *J. Electroanal. Chem.* **744**, 45 (2015)
26. M. Sahu, P. Biswas, *Nanoscale Res. Lett.* **6**, 441 (2011)
27. K. Zhang, Z.-D. Meng, W.-C. Oh, *Anal. Sci. Technol.* **23**, 225 (2010)
28. B.D. Cullity, *Elements of X-ray diffraction*. (Addison Wesley Publishing Company Inc., Massachusetts, 2001)
29. M.S. Nahar, S. Kagaya, J. Zhang, S. Kuroda, K. Hasegawa, *Mat. Sci. Semicon. Proc.* **12**, 168 (2009)
30. A.H. Dorian, C.C. Hanaor, Sorrell, *J. Mater. Sci.* **46**, 855 (2011)
31. W. Li, A.I. Frenkel, J.C. Woicik, C. Ni, S.I. Shah, *Phys. Rev. B*. **72**, 155315 (2005)
32. K. Nagaveni, M.S. Hegde, G. Madras, *J. Phys. Chem. B*. **108**, 20204 (2004)
33. I. Sang, M. Seok, S. Kim, T.S. Suh, *J. Am. Ceram. Soc.* **85**, 1888 (2002)
34. W. Choi, A. Termin, M.R. Hoffmann, *J. Phys. Chem.* **98**, 13669 (1994)
35. S.H.M. Suhaimy, S.B.A. Hamid, C.W. Lai, M.R. Hasan, M.R. Johan, *Catalysts*. **6**, 167 (2016)
36. Y. Kanemitsu, M. Okano, L.Q. Phuong, Y. Yamada, *ECS J. Solid State Sci. Technol.* **7**, R3102 (2018)